



Modeling of edge cracks interaction

V. Petrova <http://orcid.org/0000-0002-9131-2469>

Voronezh State University and University of Stuttgart, Russia

veraep@gmail.com

S. Schmauder

University of Stuttgart, Germany

siegfried.schmauder@imwf.uni-stuttgart.de

A. Shashkin

Voronezh State University, Russia

shashkin@amm.vsu.ru

ABSTRACT. From experimental and theoretical investigations it is known that cracks are sensitive to geometry, e.g., to the inclination angle to the load. A small deviation of a crack from the normal direction to a tensile load causes mixed mode conditions near the crack tip which lead to deviation of the crack from its initial propagation direction. Besides, the presence of other cracks, inhomogeneities, surfaces and their interaction causes additional deformations and stresses which also have influence on the initiation of the crack propagation and on the direction of this propagation. The aim of this paper is to show the effects of the interaction of edge cracks on further crack formation. The main fracture characteristics, such as, stress intensity factors, fracture angles and critical loads are provided in this study. A series of illustrative examples is presented for different geometries of arbitrarily inclined edge cracks.

KEYWORDS. Edge cracking; Stress intensity factors; Fracture criteria; Direction of crack propagation; Shielding-amplification effects.

INTRODUCTION

Surface cracking is observed in many engineering structures, e.g., aircraft structures, turbine blades, engine components and many others, see [1, 2] for some examples and references. In everyday life we can see asphalt pavement cracking, called also as crocodile cracking [3]. The structures are subjected to different mechanical and thermal loading as well have to resist high temperature, wear and aggressive environments. Cracks can initiate from initial defects or microcracks appear during manufacturing or service. An example of multiple surface cracking is the fracture of thermal barrier coatings (TBCs), where the upper layer is usually a ceramic - the brittle material. Investigations of thermal barrier coatings show that heating and then subsequent cooling of the coating causes the surface to experience a tensile stress leading to surface cracking [4].



There is abundant experimental results (e.g., [4-6]) showing that when TBCs are subjected to thermal shock, multiple cracks occur at the ceramic surface. Besides, the crack patterns strongly depend on the microstructure of the materials and on the type of loading.

Numerous investigations are devoted to different types of fracture including surface fracture. In previous papers of the authors [7-10] the fracture of FGM/homogeneous bimaterials (an infinite medium) under thermal and mechanical loadings were investigated, besides, in [11] some results for edge cracks in FGM/homogeneous structures (a semi-infinite medium) were obtained in the frame of the approach used in [7-10]. The results show that the fracture of materials (both composites and homogeneous) is significantly affected by a complex crack interaction mechanism, e.g., interacting cracks can enhance or suppress the propagation of each other.

During further studying of the fracture of functionally graded coatings on a homogeneous substrate and the preparation of the results for the influence of material non-homogeneity on surface fracture it became clear that a classical problem for edge cracks interaction is still not well examined. Before presenting the results for more complicated cases of non-homogeneous materials (FGMs, bimaterials, and others), modeling of the interaction of edge cracks should be done for a homogeneous medium.

From experimental and theoretical investigations it is known that cracks are sensitive to geometry, e.g., to the inclination angle to the load. A small deviation of a crack from the normal direction to a tensile load causes mixed mode conditions near the crack which lead to deviation of the crack from its initial propagation direction. Besides, the presence of other cracks, inhomogeneities, surfaces and their interaction causes additional deformations and stresses which are also influenced on the initiation of the crack propagation and on the direction of this propagation. That is, the picture of the fracture with respect to the crack pattern for a system of arbitrary inclined edge cracks will be different from the picture of regularly distributed cracks, e.g., for periodically distributed equal (and non-equal) cracks, this case was often studied, see [12-14].

The goal of this paper is to show the effects of the interaction of edge cracks on further fracture formation. The main fracture characteristics, such as, stress intensity factors, fracture angles and critical loads are provided for this study. A series of illustrative examples is presented for different geometries of arbitrarily inclined edge cracks.

PROBLEM FORMULATION AND ASSUMPTIONS

The geometry of the problem is presented in Fig. 1 a. A homogeneous half-medium contains pre-existing edge cracks inclined arbitrarily on angles β_n to the surface. A Cartesian coordinate system (x, y) has x -axis along the boundary of the half-plane, and local coordinate systems (x_k, y_k) are attached to each crack. The lengths of the cracks are $2a_n$, and the midpoint coordinates are $z_n^0 = x_n^0 + iy_n^0$ ($i = \sqrt{-1}$ is imaginary unity). The homogeneous medium is subjected to tension p applied parallel to the free surface.

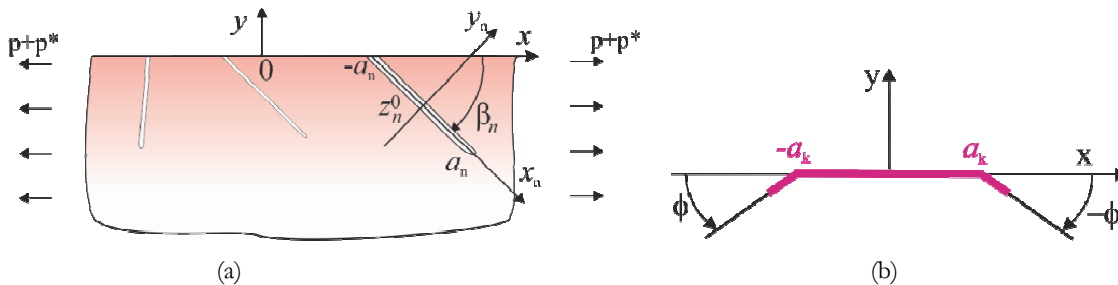


Figure 1: (a) Edge cracks inclined arbitrarily with an angle β_n to the surface of the medium. a_n – a half length of n -th crack, $z_n^0 = x_n^0 + iy_n^0$ – the crack midpoint coordinate. (b) The angle ϕ of crack deflection (the fracture angle).

The problem is solved by using the method of singular integral equations. The cracks are modeled by displacement jumps on the crack faces and unknown functions in this formulation are the derivatives of displacement jumps

$$g'_n(x) = \frac{2\mu}{i(\kappa+1)} \frac{\partial}{\partial x} ([u_n] + i[v_n]) \quad (1)$$



Here $[u_n]$ and $[v_n]$ are shear and vertical displacement jumps, respectively, on the n -th crack line, $\mu = E/2(1+\nu)$ is the shear modulus, E - Young's modulus, ν - Poisson's ratio, $\kappa = 3-4\nu$ for the plane strain state and $\kappa = (3-\nu)/(1+\nu)$ for the plane stress state.

For arbitrary located cracks in a half-plane the system of singular integral equations is written as [15, 16]

$$\int_{-a_n}^{a_n} \frac{g'_n(t)dt}{t-x} + \sum_{\substack{k=1 \\ k \neq n}}^N \int_{-a_k}^{a_k} [g'_k(t)R_{nk}(t,x) + \overline{g'_k(t)}S_{nk}(t,x)]dt = \pi p_n(x), \quad |x| < a_n, \quad n = 1, 2, \dots, N \quad (2)$$

An overbar ($\bar{\dots}$) is the complex conjugate. N is number of cracks.

The method of superposition was used in deriving of Eq. (2) where the loads at infinity are reduced to the corresponding loads on the crack faces. The functions p_n in the right side of Eq. (2) are these loadings, and in the case of a homogeneous half-plane under tension p they are written as

$$p_n = \sigma_n - i\tau_n = p(1 - \exp(-2i\alpha_n))/2 \quad (n = 1, 2, \dots, N) \quad (3)$$

with $\alpha_n = -\beta_n$ (see Fig. 1 a).

If a non-homogeneous medium is considered, e.g., a functionally graded structure with continuous gradation of the thermo-mechanical properties with the coordinate y , and this structure is cooled, then tensile residual stresses are arising due to mismatch in the coefficients of thermal expansion [4, 14]. The influence of this inhomogeneity can be accounted via continuously varying residual stresses p^* which are written as follows [14]:

$$p^* = \sigma_{xx}^T(y) = [\alpha_t(y) - \alpha_{t0}] \Delta TE$$

This function is added to the right side of Eq. (2). It should be noted, that in this case we also have the problem for a half-plane under tension.

NUMERICAL SOLUTION, STRESS INTENSITY FACTORS

The solution of singular integral equations (Eq. 2) is obtained by a numerical method which is based on Gauss-Chebyshev quadrature. The method is similar to the method presented by Erdogan and Gupta [17], but we will follow the version formulated in [15, 16].

The equations (2) are rewritten in dimensionless form with the non-dimensionless coordinates $\xi = t/a_k$ and $\eta = x/a_n$, where $2a_k$ is a length of the k -th crack. The unknown function $g'_n(\eta)$ consists of a function $u_n(\eta)$ (a bounded continuous function in the segment $[-1, 1]$) and the weight function $1/\sqrt{1-\eta^2}$, that is,

$$g'_n(\eta) = u_n(\eta)/\sqrt{1-\eta^2} \quad (4)$$

For edge cracks the function $g'_n(\eta)$ possess a singularity less than $1/\sqrt{1+\eta}$ at the edge point $\eta = -1$ and this condition is accounted as [15, 16]

$$u_n(-1) = 0 \quad (5)$$

In spite of the exact singularity at the edge points is not taking into account, the numerical results have shown good accuracy [15, 16].

Using Gauss's quadrature formulae for the regular and singular integrals the integral equations are reduced to the following system of $N \times M$ (N – number of cracks, M – number of nodes) algebraic equations



$$\frac{1}{M} \sum_{m=1}^M \sum_{k=1}^N [u_k(\xi_m) R_{nk}(\xi_m, \eta_r) + \overline{u_k(\xi_m)} S_{nk}(\xi_m, \eta_r)] = \pi p_n(\eta_r), \quad (6)$$

$$\sum_{m=1}^M (-1)^m u_n(\xi_m) \tan \frac{2m-1}{4M} \pi = 0 \quad (n=1,2, \dots, N; r=1,2, \dots, M-1) \quad (7)$$

with

$$\xi_m = \cos \frac{2m-1}{2M} \pi \quad (m=1,2,\dots,M); \quad \eta_r = \cos \frac{\pi r}{M} \quad (r=1,2,\dots,M-1)$$

M is the total number of discrete points of the unknown functions $u_n(\eta)$ within the interval (-1,1). Applying the conjugate operation to the system (6) additional $N \times M$ equations are obtained, i.e. $2N \times M$ equations should be solved, where N is the number of cracks.

Eq. (7) is obtained from the condition (5) and the interpolation formula for the functions $u_n(\eta)$:

$$u_n(\eta) = \frac{2}{M} \sum_{m=1}^M u_n(\xi_m) \sum_{r=0}^{M-1} T_r(\xi_m) T_r(\eta) - \frac{1}{M} \sum_{m=0}^M u_n(\xi_m). \quad (8)$$

Here T_r are Chebyshev polynomials of the first kind. Inserting (8) into Eq. (4) the derivative of displacement jumps on the crack lines are obtained and then the displacement jumps can be derived by integrating the function (4) with (8).

The stress intensity factors (SIFs) are calculated according to the following formula

$$\begin{aligned} K_{In} - iK_{II,n} &= -\sqrt{a_n} u_n(+1) \\ &= p_n \sqrt{a_n} \frac{1}{M} \sum_{m=1}^M (-1)^m u_n(\xi_m) \cot \frac{2m-1}{4M} \pi \quad (n = 1, 2, \dots, N). \end{aligned} \quad (9)$$

CRITICAL LOADS, FRACTURE ANGLES

For general crack problems the stress intensity factors are both nonzero, i.e. mixed-mode conditions are in the vicinity of cracks. For this mixed-mode case the cracks deviate from their initial propagation direction. For the prediction of the crack growth and direction of this growth a fracture criterion should be applied. Using the maximum circumferential stress criterion (see [18] and for references [15, 16]) the direction of the initial crack propagation (Fig. 1 b) is evaluated as

$$\phi = 2 \arctan \left[\left(K_I - \sqrt{K_I^2 + 8K_{II}^2} \right) / 4K_{II} \right] \quad (10)$$

and the critical stresses can be calculated from the expression

$$\cos^3(\phi/2)(K_I - 3K_{II} \tan(\phi/2)) = K_{Ic} / \sqrt{\pi}. \quad (11)$$

Here K_{Ic} is the fracture toughness of the material. The critical stresses are given as

$$p_{cr} = P_{cr} / p_0 = P_{cr} / (K_{Ic} / \sqrt{2\pi a}) = 1 / [\cos^3(\phi/2)(k_I - 3k_{II} \tan(\phi/2))]. \quad (12)$$

Here $k_{I,II}$ are non-dimensional SIFs



$$k_{I,II} = K_{I,II} / K^0, \quad K^0 = p\sqrt{2a} \quad (15)$$

and $p_0 = K_L / (2\pi a)^{1/2}$ is critical load for a single crack in a material with the fracture toughness K_L .

For the system of cracks the fracture starts from the crack tip where P_{cr} is minimal, i.e. $\min_k [P_{cr(k)} / p_0]$.

RESULTS AND DISCUSSION

Some examples for edge crack interaction is investigated and presented here for homogeneous materials. The verification of the method and the numerical outcomes has been done in [11], where the results for some special cases were compared with the results for SIFs for a single inclined edge crack cited in [19] and with SIFs for periodic edge cracks cited in [20].

The tensile loading p is applied parallel to the boundary and on the crack lines we have the loading Eq. (3). The non-dimensional stress intensity factors Mode I and Mode II ($k_{I,II}$) are defined by Eqs. (9) and (15). Non-dimensional k_I for a single edge crack normal to the surface is equal to $k_I = 1.12$ and SIF k_{II} is $k_{II} = 0$.

The non-dimensional distances $d = \hat{d} / a$ between the cracks are $d = 1, 2, 4, 6$, $a = \max_k a_k$ and we remind that $2a_k$ is the size of the k -th crack. After obtaining SIFs the fracture angles ϕ are calculated by Eq. (10) and critical loads p_{cr} by Eq. (12).

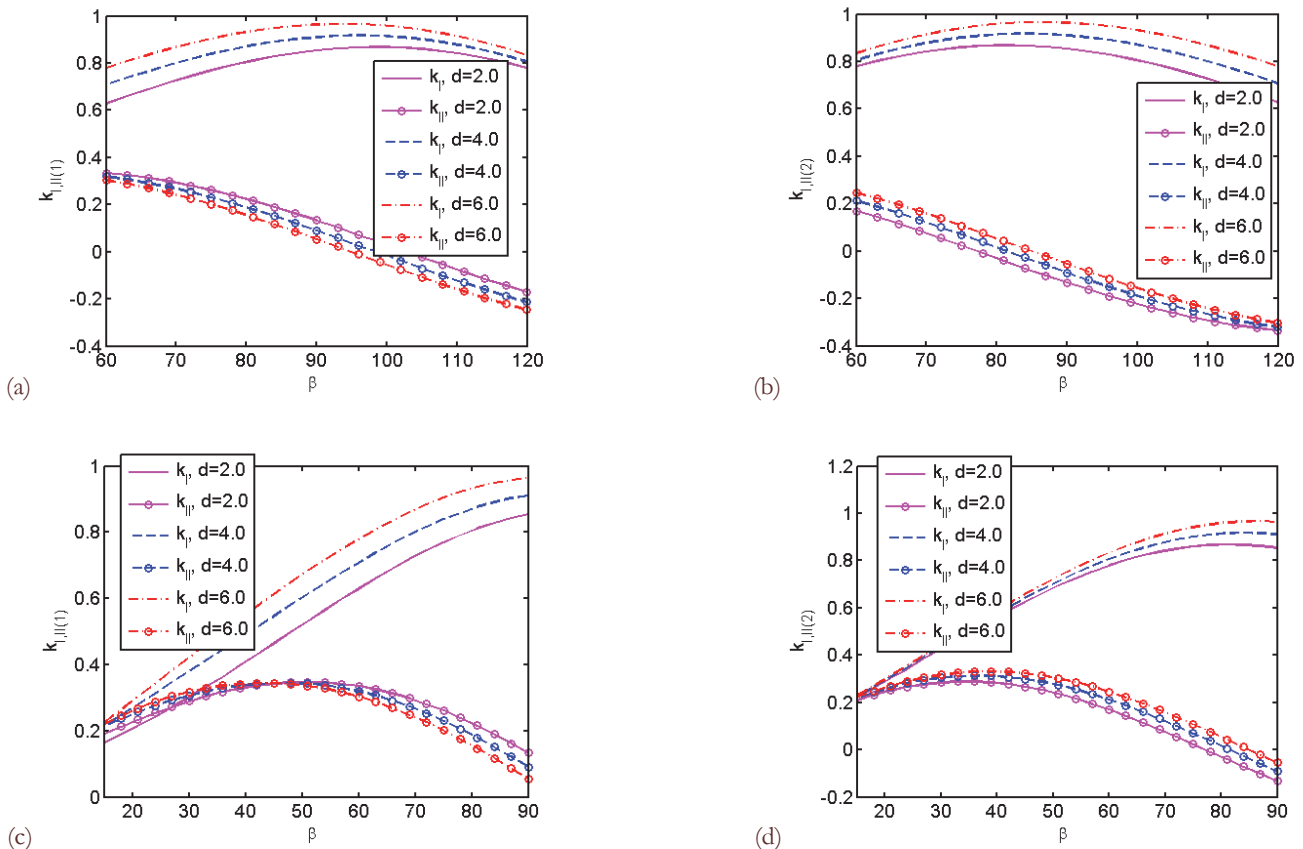


Figure 2: Stress intensity factors k_I and k_{II} as functions of the inclination angle $\beta = \beta_n$ of the edge cracks to the surface for different distances d between the cracks: (a) for crack 1 ($60^\circ \leq \beta \leq 120^\circ$), (b) for crack 2 ($60^\circ \leq \beta \leq 120^\circ$), (c) for crack 1 ($15^\circ \leq \beta \leq 90^\circ$), (d) for crack 2 ($15^\circ \leq \beta \leq 90^\circ$). Two equal edge cracks.

Two arbitrary inclined cracks

Figs. 2, 5 and 8 show the SIFs $k_{I,II}$, Figs. 3, 6 and 9 – the fracture angles, and Figs. 4, 7 and 10 – the critical loads as functions of inclination angles of the two edge cracks to the surface and for different distances d .

It is observed that for all angles β SIF k_I increases with increasing the distance d between the cracks and k_I tends to the value for a single edge crack, e.g., to $k_I = 1.12$ and $k_{II} = 0$ at $\beta = 90^\circ$. Besides, for all parameters of the problem the values of k_I are smaller than the values of k_I for a single crack (Figs. 2, 5 and 8). That is, the shielding effect is observed, which is known for parallel cracks under tensile load normal to the crack lines.

Figs. 2–4 present results for two equal edge cracks inclined arbitrarily to the surface with the same angle $\beta = \beta_n$ ($n=1, 2$). Stress intensity factors k_I and k_{II} as functions of the inclination angle β are presented for the angles $60^\circ \leq \beta \leq 120^\circ$ in Figs. 2 a, b and for $15^\circ \leq \beta \leq 90^\circ$ in Figs. 2 c, d and for different distances d between the cracks.

In the interval $60^\circ \leq \beta \leq 120^\circ$ a small variation of the magnitude of k_I with β is observed (Fig. 2 a, b), but in the interval $15^\circ \leq \beta \leq 60^\circ$ for the small inclinations angles this variation is significant (Figs. 2 b, c). k_I is increased from 0.2 to 0.99 for $15^\circ \leq \beta \leq 90^\circ$ (for $d=2$) and then decreased for $90^\circ \leq \beta \leq 120^\circ$.

SIFs k_{II} are mostly nonzero, the absolute values of k_{II} are greater than k_I , and k_{II} is monotonically decreased for $60^\circ \leq \beta \leq 120^\circ$ (Fig. 2 a, b) and increased for $15^\circ \leq \beta \leq 45^\circ$ (Figs. 2 b, c).

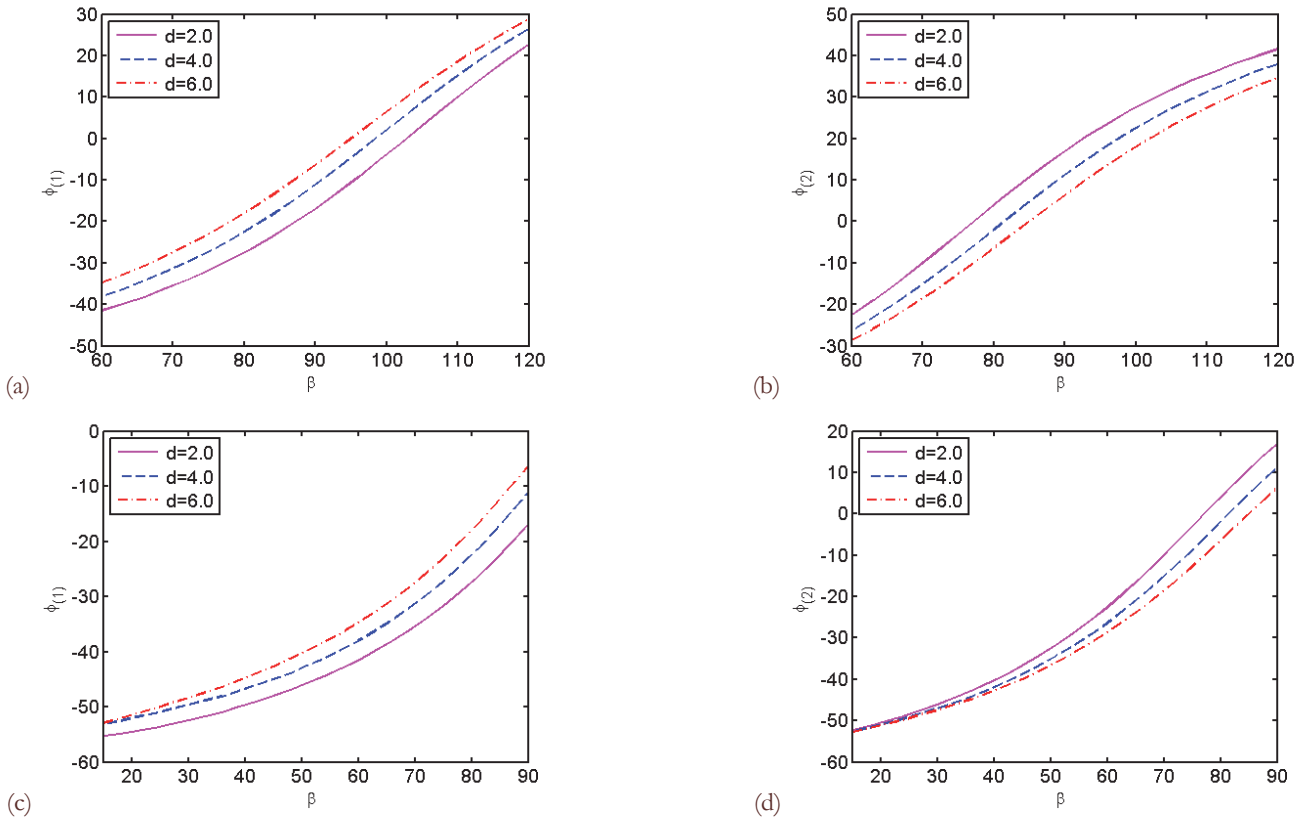


Figure 3: Fracture angles $\phi_{(1)}$ and $\phi_{(2)}$ as functions of the inclination angle $\beta = \beta_n$ of the edge cracks to the surface for different distances d between the cracks: (a) for crack 1 ($60^\circ \leq \beta \leq 120^\circ$), (b) for crack 2 ($60^\circ \leq \beta \leq 120^\circ$), (c) for crack 1 ($15^\circ \leq \beta \leq 90^\circ$), (d) for crack 2 ($15^\circ \leq \beta \leq 90^\circ$). Two equal edge cracks.

The fracture angles ϕ for two edge cracks are presented in Figs. 3, strong influence of the inclination angles β on the fracture angles ϕ is observed. For all β fracture angles ϕ are increased and changed the sign from negative to positive at $\beta \approx 103^\circ$ (crack 1) and at $\beta \approx 77^\circ$ (crack 2) for $d=2$, for larger distances d these points are shifted towards $\beta \approx 99^\circ$ (crack 1) and $\beta \approx 81^\circ$ (crack 2) for $d=4$ (Fig. 3 a, b). These changes of sign mean the changes of direction of the crack propagation.

Fig. 4 shows results for the non-dimensional critical loads for crack 1 and for both cracks in Fig. 4 b ($60^\circ \leq \beta \leq 120^\circ$) and 4 d ($15^\circ \leq \beta \leq 90^\circ$). The larger the distance between the cracks – the less the p_{cr} , i.e. the material becomes weaker with respect to fracture resistance. What crack starts to propagate first depends on the inclination angle, for $62^\circ \leq \beta \leq 90^\circ$ $p_{cr(1)} < p_{cr(2)}$ and the crack 1 propagates first and for $90^\circ < \beta < 118^\circ$ the crack 2 will be starting first (Fig. 4 b). For small angles $15^\circ \leq$



$\beta \leq 62^\circ$, where the crack 2 is close to the free surface, $p_{\sigma(2)} < p_{\sigma(1)}$ and the crack 2 will propagate first (Fig. 4 d). The opposite picture for critical loads and crack propagation is observed for other values of β .

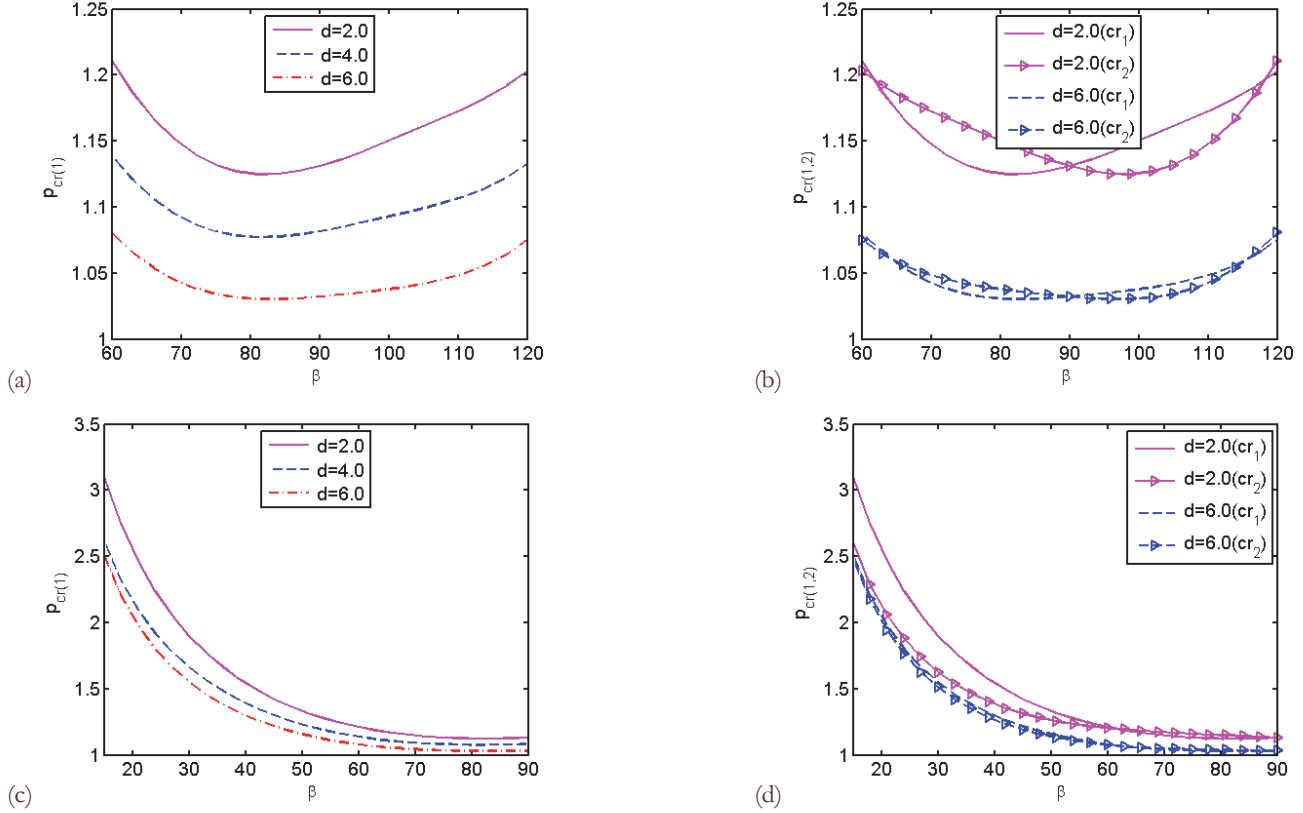


Figure 4: The non-dimensional critical load p_{σ} as function of the inclination angle $\beta=\beta_n$ for two equal edge cracks for different distances d between the cracks: (a) for crack 1 ($60^\circ \leq \beta \leq 120^\circ$), (b) for two cracks ($60^\circ \leq \beta \leq 120^\circ$), (c) for crack 1 ($15^\circ \leq \beta \leq 90^\circ$), (d) for two cracks ($15^\circ \leq \beta \leq 90^\circ$). Two equal edge cracks.

Another case for two cracks with different sizes is presented in Figs. 5–7. It is assumed that non-dimensional crack sizes (a_k/a , $a = \max_k a_k$) are $a_1=1$ and $a_2=0.5$, and as previously $\beta=\beta_n$ ($n = 1, 2$). It is observed, that distance d has small influence on the fracture parameters for the crack 1, i.e. SIFs, fracture angles and critical loads are nearly the same for the considered d -values $d=2, 4$ and 6 (Figs. 5 a, c, 6 a, c and 7 a, c). However, the influence of d on the crack 2 is strong (Figs. 5 b, d, 6 b, d and 7 b, d). Both cracks are sensitive to the inclination angle β . The influence of β on the SIFs and the fracture angles for the crack 1 are similar to the previous case and are differ from the previous for the crack 2 (see Figs. 5 and 6).

The critical loads are presented in Fig. 7. For two parallel cracks with different sizes the larger crack (crack 1) will propagate first because of $p_{\sigma(1)} < p_{\sigma(2)}$ for all angles β (Fig. 7 e, f). For close locate cracks the critical load $p_{\sigma(2)}$ for the smaller crack is much larger than $p_{\sigma(1)}$, Fig. 7. For far distances between the cracks (e.g., for $d=6$) the difference between the critical loads becomes less and the cracks have equal chances for propagation.

Figs. 8 – 10 show fracture parameters for two unequal cracks with sizes $a_1=1$ and $a_2=0.5$ (as previously), but with the fixed inclination angle $\beta_1=90^\circ$ and varied β_2 , for the distances $d = 1, 2, 4, 6$. For the fixed crack 1 the SIFs $k_{I(1)}$ and $k_{II(1)}$ are nearly the same as for the corresponding single edge crack, Fig. 8 a, and the fracture angle $\phi_{(1)}$ is small, Fig. 9 a. For the arbitrary inclined crack 2 the fracture angle $\phi_{(2)}$ is increased with increasing inclination angle β_2 and changed the sign from minus to plus. The critical loads are depicted in Fig. 10. The influence of the distance d on $p_{\sigma(1)}$ is not large, the maximal difference is 3.5% between the values of $p_{\sigma(1)}$ for $d=1$ and $d=6$, Fig. 10 a. A comparison of the critical loads for two cracks shows that the crack 1 will propagate first because of $p_{\sigma(1)} < p_{\sigma(2)}$, Fig. 10 b.

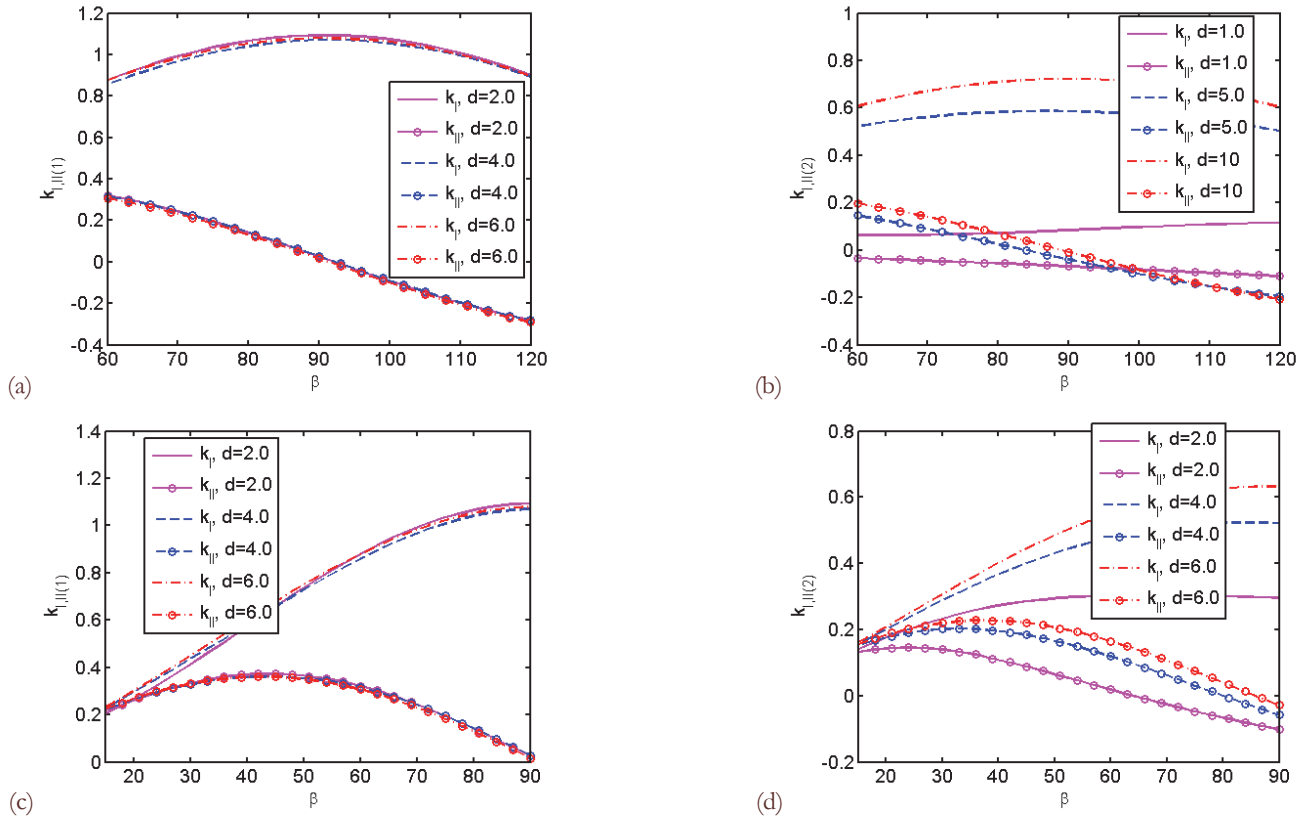


Figure 5: Stress intensity factors k_I and k_{II} as function of the inclination angle $\beta=\beta_n$ of the edge cracks to the surface for different distances d between the cracks: (a) for crack 1 ($60^\circ \leq \beta \leq 120^\circ$), (b) for crack 2 ($60^\circ \leq \beta \leq 120^\circ$), (c) for crack 1 ($15^\circ \leq \beta \leq 90^\circ$), (d) for crack 2 ($15^\circ \leq \beta \leq 90^\circ$). Two edge cracks with different sizes $a_1=1$ and $a_2=0.5$.

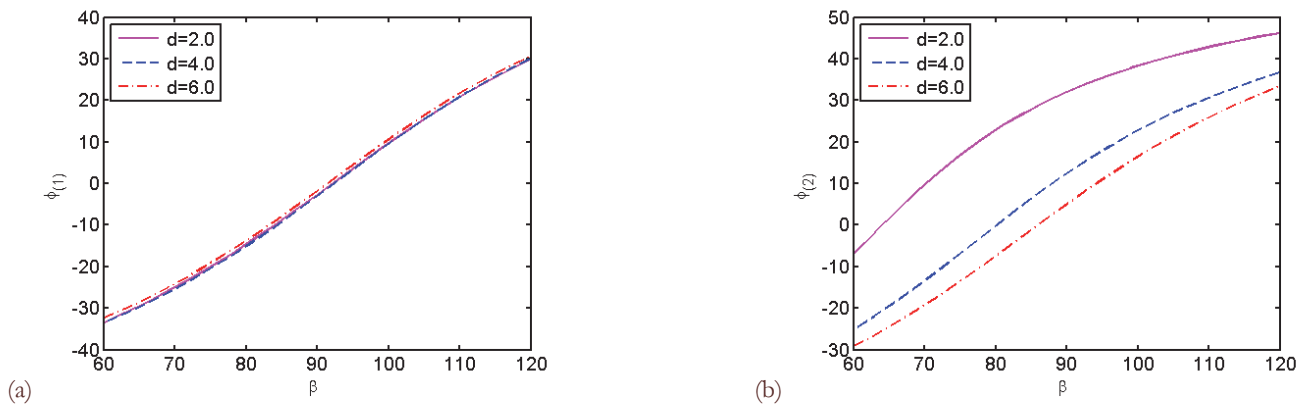


Figure 6 a, b: Fracture angles $\phi_{(1)}$ and $\phi_{(2)}$ as functions of the inclination angle $\beta=\beta_n$ of the edge cracks to the surface for different distances between the cracks: (a) for crack 1 ($60^\circ \leq \beta \leq 120^\circ$), (b) for crack 2 ($60^\circ \leq \beta \leq 120^\circ$). Two edge cracks with different sizes $a_1=1$ and $a_2=0.5$.

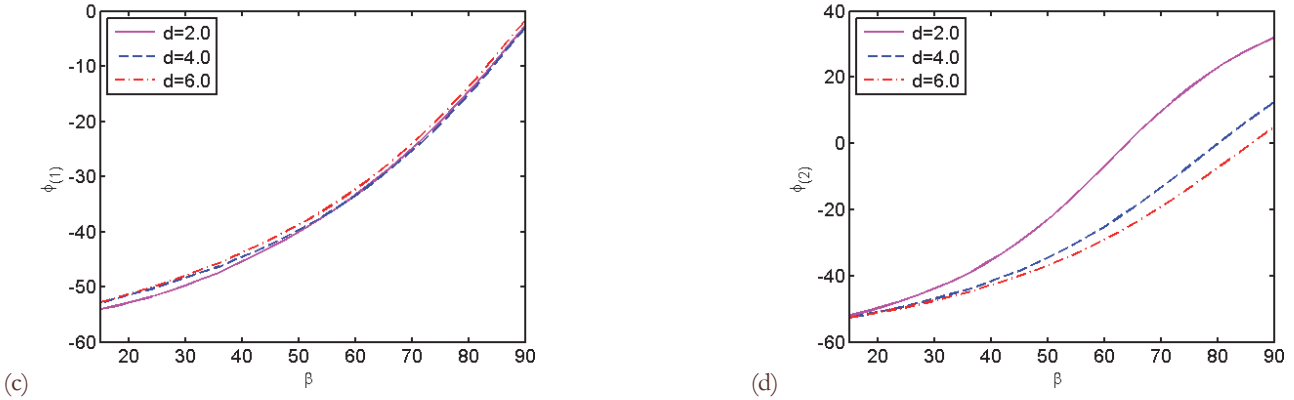


Figure 6 c, d: Fracture angles $\phi_{(1)}$ and $\phi_{(2)}$ as functions of the inclination angle $\beta=\beta_n$ of the edge cracks to the surface for different distances d between the cracks: (c) for crack 1 ($15^\circ \leq \beta \leq 90^\circ$), (d) for crack 2 ($15^\circ \leq \beta \leq 90^\circ$). Two edge cracks with different sizes $a_1=1$ and $a_2=0.5$.

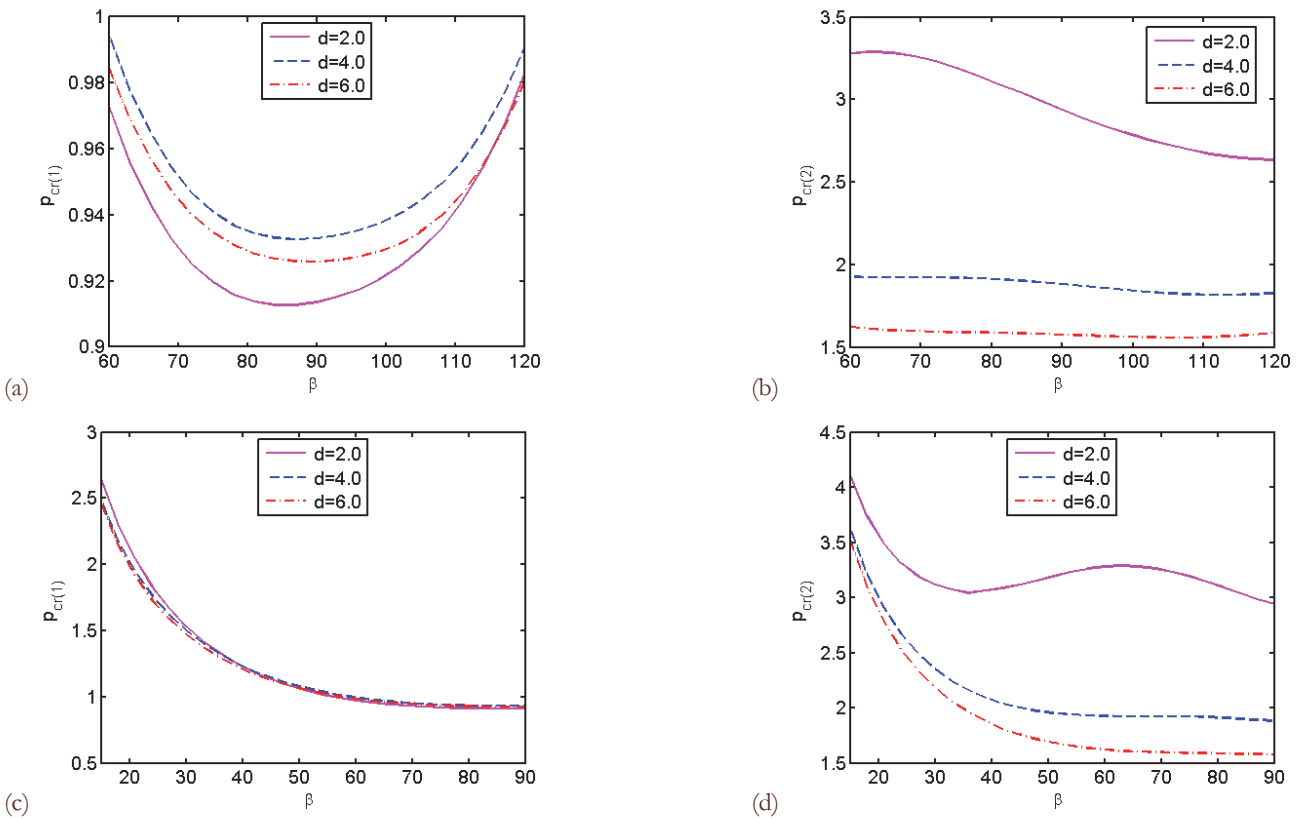


Figure 7 a-d: The non-dimensional critical load p_{cr} as function of the inclination angle $\beta=\beta_n$ for two equal edge cracks for different distances d between the cracks: (a) for crack 1 ($60^\circ \leq \beta \leq 120^\circ$), (b) for crack 2 ($60^\circ \leq \beta \leq 120^\circ$), (c) for crack 1 ($15^\circ \leq \beta \leq 90^\circ$), (d) for crack 2 ($15^\circ \leq \beta \leq 90^\circ$). Two edge cracks with different sizes $a_1=1$ and $a_2=0.5$.

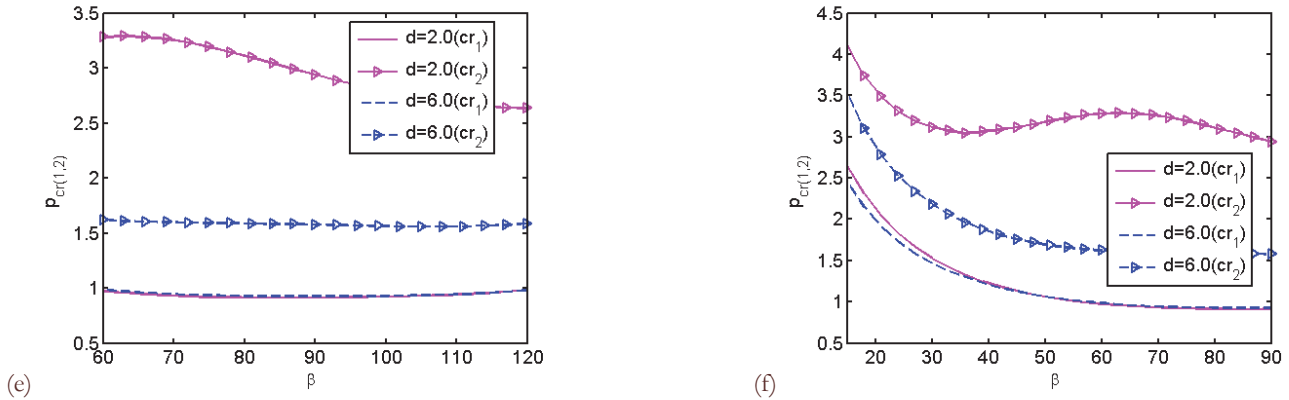


Figure 7 e, f: The non-dimensional critical load p_{cr} as function of the inclination angle $\beta=\beta_n$ for two equal edge cracks for different distances d between the cracks: (e) for cracks 1 and 2 ($60^\circ \leq \beta \leq 120^\circ$) and (f) for cracks 1 and 2 ($15^\circ \leq \beta \leq 90^\circ$). Two edge cracks with different sizes $a_1=1$ and $a_2=0.5$.

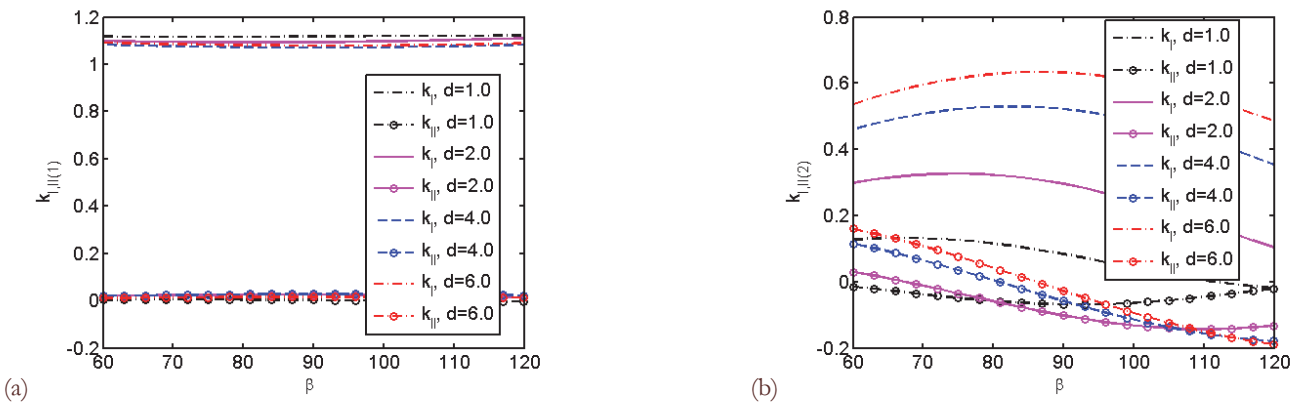


Figure 8: Stress intensity factors k_I and k_{II} as function of the inclination angle $\beta=\beta_2$ ($60^\circ \leq \beta \leq 120^\circ$) and for $\beta_1=90^\circ$ for different distances d between the cracks: (a) for crack 1, (b) for crack 2. Two edge cracks with different sizes $a_1=1$ and $a_2=0.5$.

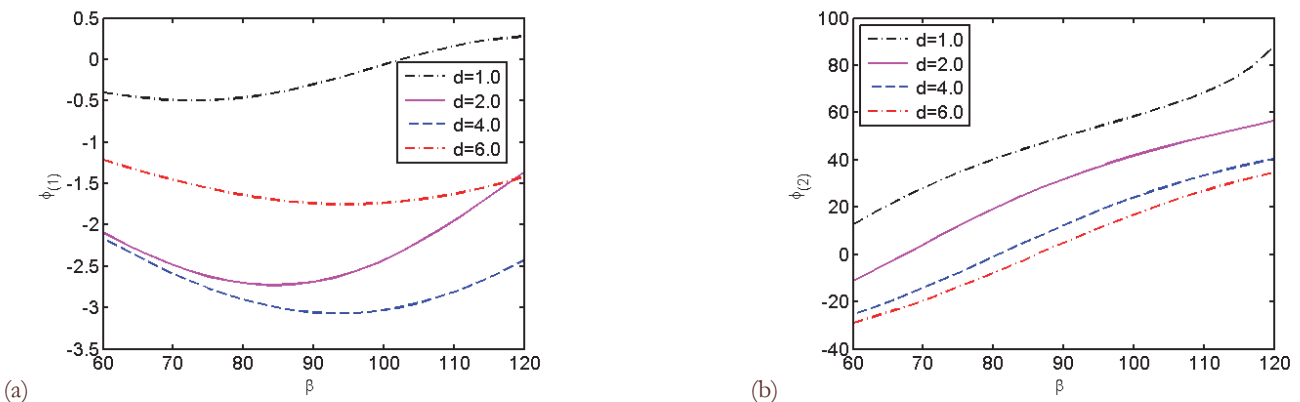


Figure 9: Fracture angles $\phi_{(1)}$ and $\phi_{(2)}$ as functions of the inclination angle $\beta=\beta_2$ ($60^\circ \leq \beta \leq 120^\circ$) and for $\beta_1=90^\circ$ for different distances d between the cracks: (a) for crack 1, (b) for crack 2. Two edge cracks with different sizes $a_1=1$ and $a_2=0.5$.

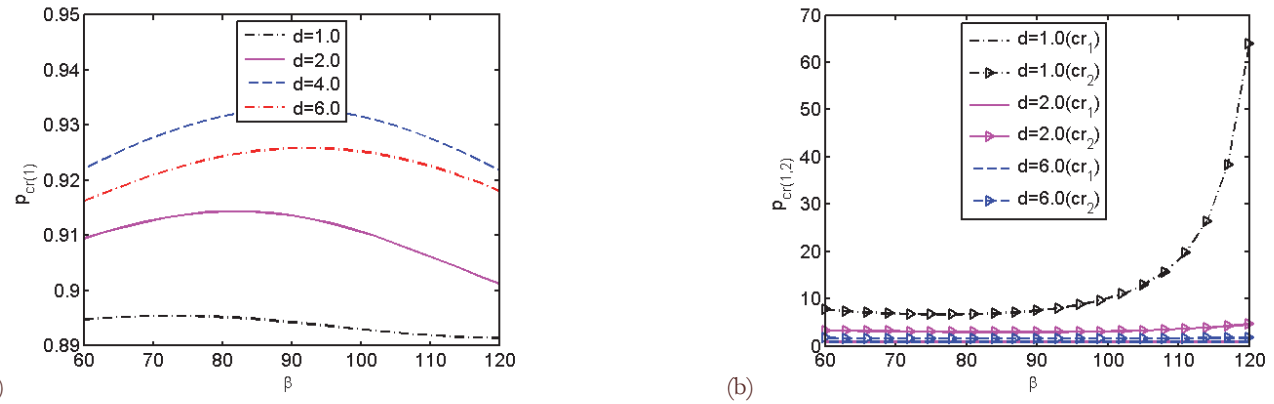


Figure 10: The non-dimensional critical load p_{cr} as function of the inclination angle $\beta=\beta_2$ ($60^\circ \leq \beta \leq 120^\circ$) and for $\beta_1=90^\circ$ for different distances d between the cracks: (a) for crack 1, (b) for cracks 1 and 2. Two edge cracks with different sizes $a_1=1$ and $a_2=0.5$.

The schemes of the direction of cracks propagation are shown in Fig. 11 for inclination angles $\beta=90^\circ$ and 60° and for different distances between the cracks. For a single edge crack with $\beta=90^\circ$ the fracture angle is equal to $\phi=0^\circ$. It is shown in Fig. 11 a the both cracks will change the direction of the propagation and the fracture angles are larger for closely located cracks for $d=2$ than for the distances $d=4$ and 6 between the cracks where the fracture angles are $\phi=12^\circ$ and 8° . The results for two unequal cracks are shown in Fig. 11 c. The crack 1 slightly deviates away from crack 2 if the distance is $d=2$ and will propagate straight for far distances between the cracks. At the same time the influence of the big crack on the propagation direction of the small is rather strong. Fig. 11 d show the fracture angles for the cracks inclined under the angle $\beta=60^\circ$. For a single edge crack with $\beta=60^\circ$ the fracture angle is equal to 31° . The difference in the fracture angles due to their interaction is dependent on the distance between the cracks and the size of these cracks.

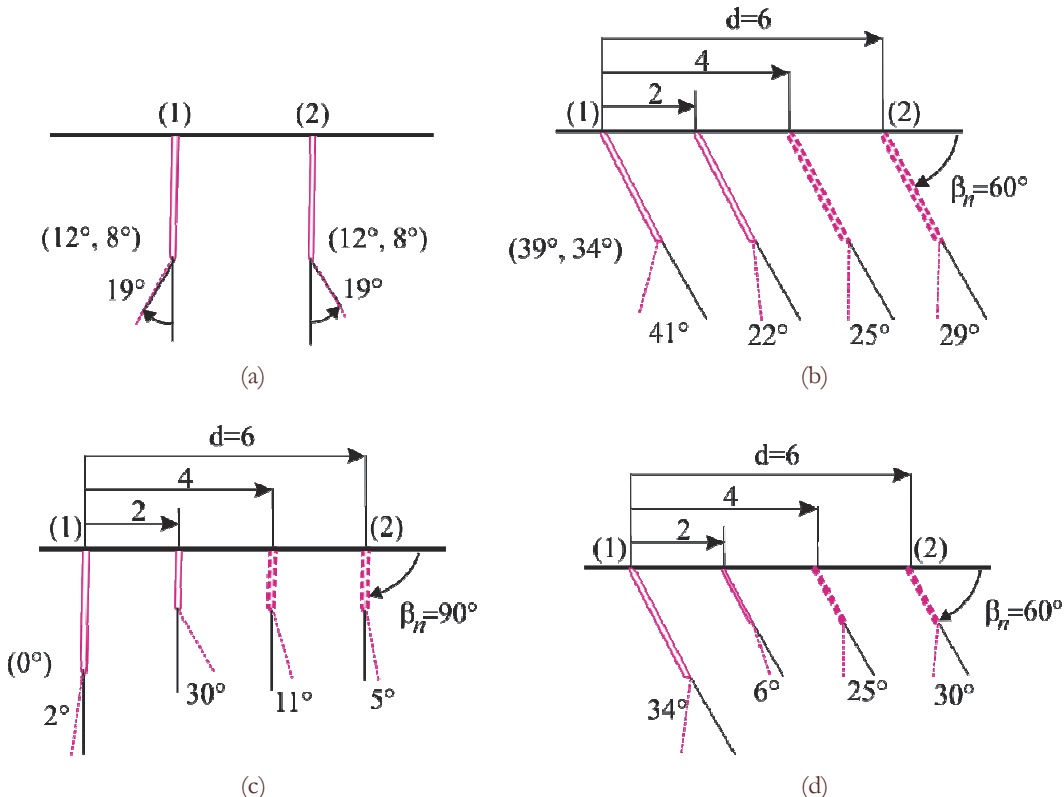


Figure 11: Schematic representation of the fracture angles: (a) and (b) for two equal cracks with inclined angles $\beta=90^\circ$ and 60° correspondingly; (c) and (d) for two crack of sizes $a_1=1$ and $a_2=0.5$ and with inclined angles $\beta=90^\circ$ and 60° .



As shown in Figs. 3, 6 and 9, there are crack configurations for which cracks are not deviating from their initial direction, i.e. $\phi = 0$. Tab. 1 presents such results, e.g., crack 1 has the fracture angle $\phi = 0^\circ$ for $\beta_{1,2}=103^\circ$, the crack 2 for this case has $\phi = 30^\circ$. For close located cracks (for $d=1$) with $\beta_{1,2}=90^\circ$ the crack interaction gives the fracture angles $(\phi_1, \phi_2)=(0^\circ, 50^\circ)$, see column first in the Tab. 1. For a single edge crack for $\beta=90^\circ$ the crack has the zero fracture angle.

d	$d=1$	$d=2$	$d=4$	$d=6$		
β, ϕ (degree)	$\beta_1 = \beta_2$	(ϕ_1, ϕ_2)	$\beta_1 = \beta_2$	(ϕ_1, ϕ_2)	$\beta_1 = \beta_2$	(ϕ_1, ϕ_2)
$(a_1, a_2)=(1.0, 1.0)$	-	-	103	$(0, 30)$	99	$(0, 20)$
	-	-	77	$(-30, 0)$	81	$(-20, 0)$
$(a_1, a_2)=(1.0, 0.5)$	90	$(0, 50)$	90	$(0, 33)$	90	$(0, 10)$
	not exist	-	63	$(-30, 0)$	80	$(-18, 0)$
					90	$(0, 3)$
					86	$(-10, 0)$

Table 1: Some cases for crack configurations for which cracks are not deviating from their initial direction.

Three arbitrary inclined cracks

Consider the case for three arbitrary inclined edge cracks. Figs. (10)-(12) are for the cracks with same sizes and Figs. (15)-(22) for different sizes, i.e. $a_1=1$, $a_2=0.5$ and $a_3=0.5$.

Fig. 12 shows the SIFs k_I and k_{II} , Fig. 13 – the fracture angles, Figs. 14 – the critical loads as functions of inclination angle $\beta=\beta_n$ ($n=1, 2, 3$) for three interacting edge cracks of the same size. The results are presented for the crack 2 (the middle crack), for other cracks 1 and 3, the plots are similar to the previous case for two interacting cracks, Fig. 2. The distances between the cracks are equal (see Fig. 21 a) and the calculation is performed for $d=2, 4$ and 6 .

The curves for k_I for all three cracks are similar, but the values for k_I are different $k_{I(2)} < k_{I(1,3)}$ for all β and d . The influence of the distance on the k_I is stronger for the crack 2, than for cracks 1 and 3. The SIF $k_{II(2)}$ is also less than k_{II} for cracks 1 and 3 and have small dependence on the distance d . The strong shielding effect is observed for the middle crack 2.

The fracture angles ϕ are presented in Fig. 13 only for the crack 2, for cracks 1 and 3 they are nearly the same as in Fig. 3 for two cracks. Some selected cases for directions of crack propagation are shown in Fig. 21 a, b. The influence of the inclination angle on the fracture angles is evident as well as the influence of interaction between the cracks.

Fig. 14 shows the non-dimensional critical loads for the three equal cracks, Fig. 14 a for $60^\circ \leq \beta \leq 120^\circ$ and Fig. 14 b for $15^\circ \leq \beta \leq 90^\circ$. The critical loads $p_{cr(1,3)} < p_{cr(2)}$ for all parameters, hence the outer cracks 1 and 3 will start to propagate first.

Some results are presented in Figs. 15 – 17 for cracks with different sizes $a_1=1$ and $a_2=a_3=0.5$ and equally inclined to the surface. Fig. 15 shows SIFs for cracks 2 and 3, the curves for the crack 1 (the bigger crack) are similar to the curves for the crack 1 in Fig. 5 a, c. $k_{I(2)} < k_{I(3)}$ and $k_{I(2,3)} < k_{I(1)}$ for all parameters, that is, the maximum shielding effect is observed for the crack 2. The SIFs k_{II} are small (close to zero) and their absolute values for cracks 2 and 3 are less than for crack 1.

The fracture angles ϕ are presented in Fig. 16 for the small cracks 2 and 3 and for the crack 1 the curves are similar to the curves in Fig. 6 a, c. Some schemes for the direction of the crack propagation are presented in Fig. 21 c, d.

The non-dimensional critical loads for the three unequal cracks are presented in Fig. 17. $p_{cr(2)} >> p_{cr(1,3)}$ for $60^\circ \leq \beta \leq 120^\circ$ and for $15^\circ \leq \beta \leq 90^\circ$ ($d=2$), besides $p_{cr(2)} > p_{cr(3)} > p_{cr(1)}$. The larger crack will propagate first.

The last case for the three edge cracks is presented in Figs. 18 – 22. The sizes of cracks are equal, the first crack is inclined with $\beta_1=90^\circ$ and $\beta_{2,3}=\beta$ are varied. The SIFs are shown in Fig. 18. The dependence of k_I and k_{II} with changing β are similar as for two interacting cracks, Fig. 8, but the values of k_I are smaller for the three crack case for all parameters. The fracture angles are presented in Fig. 19. The dependence of ϕ with β for crack 3 is similar to the two-crack case in Fig. 9 b. The fracture angles for the crack 1 ($\beta_1=90^\circ$) are larger than for the crack 1 interacting with only one crack, Fig. 9 a, and they are much smaller than the values ϕ for cracks 2 and 3, as expected, because of a single crack with $\beta_1=90^\circ$ don't change the direction of propagation.

Fig. 20 shows the non-dimensional critical loads for this case of interacting cracks, Fig. 20 a for the crack 1 and Fig. 20 b is for three cracks. The critical load for the middle crack 2 is much larger than for other cracks for all β values. For inclinations $\beta_{2,3}=\beta$ close to 90° ($88^\circ \leq \beta \leq 102^\circ$), when the three cracks nearly parallel, $p_{cr(1)} = p_{cr(3)}$, so that the cracks 1 and 3 will start to propagate first, for other inclination angles the weaker is the crack 1.

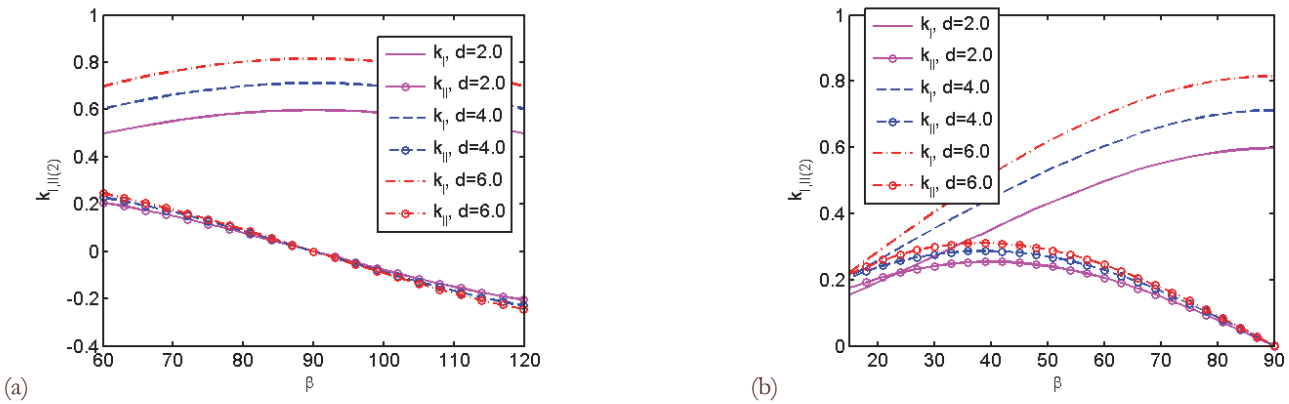


Figure 12: Stress intensity factors k_I and k_{II} as functions of the inclination angle $\beta=\beta_n$ of the edge cracks to the surface for different distances d between the cracks: (a) for crack 2 ($60^\circ \leq \beta \leq 120^\circ$) (b) for crack 2 ($15^\circ \leq \beta \leq 90^\circ$) (SIFs for cracks 1 and 3 are similar as in Figs. 2 a, b for two crack). Three equal edge cracks.

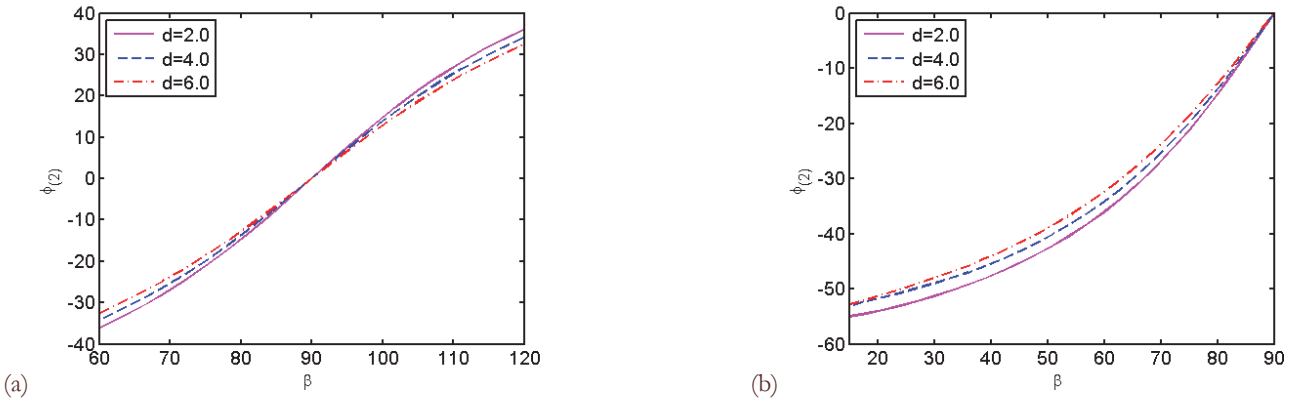


Figure 13: Fracture angles $\phi_{(2)}$ as functions of the inclination angle $\beta=\beta_n$ of the edge cracks to the surface for different distances d between the cracks: (a) for crack 2 ($60^\circ \leq \beta \leq 120^\circ$) and (b) for crack 2 ($15^\circ \leq \beta \leq 90^\circ$). (The fracture angles ϕ for cracks 1 and 3 are similar as in Figs. 3 a, b for two crack.) Three equal edge cracks.

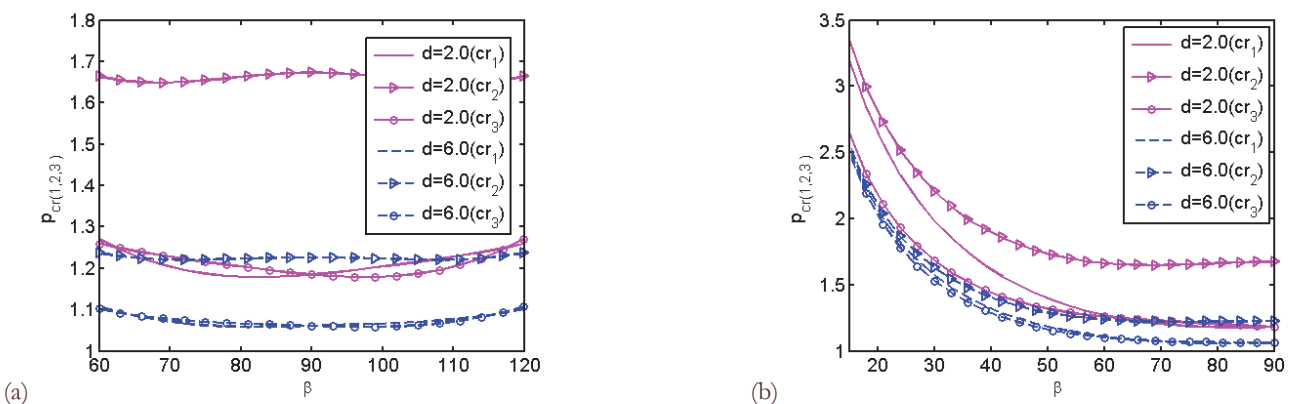


Figure 14: The non-dimensional critical load p_{cr} as function of the inclination angle $\beta=\beta_n$ for equal edge cracks for different distances d between the cracks: (a) for three cracks ($60^\circ \leq \beta \leq 120^\circ$), (b) for three cracks ($15^\circ \leq \beta \leq 90^\circ$).

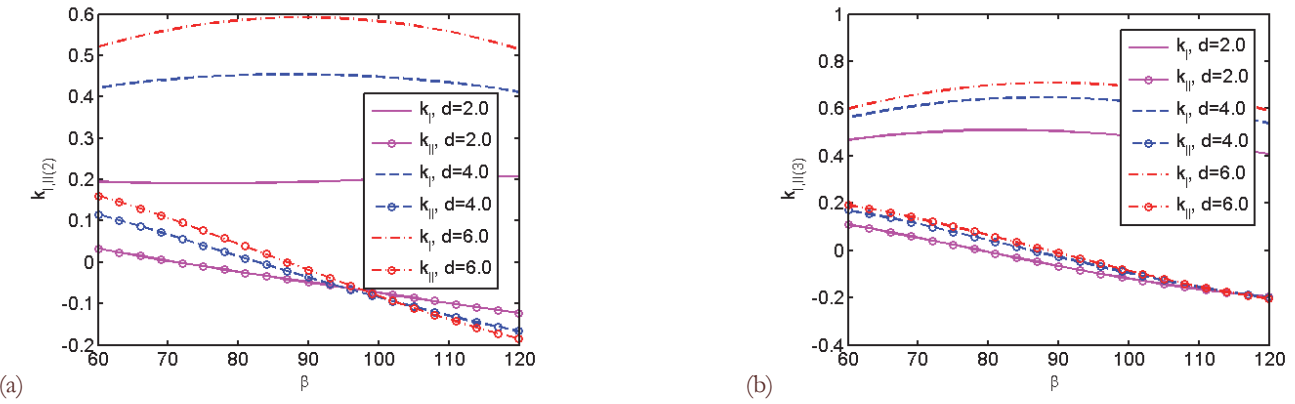


Figure 15: Stress intensity factors k_I and k_{II} as function of the inclination angle $\beta=\beta_n$ of the edge cracks to the surface for different distances d between the cracks: (a) for crack 2 ($60^\circ \leq \beta \leq 120^\circ$), (b) for crack 3 ($60^\circ \leq \beta \leq 120^\circ$). Three edge cracks with different sizes $a_1=1$ and $a_2=a_3=0.5$.

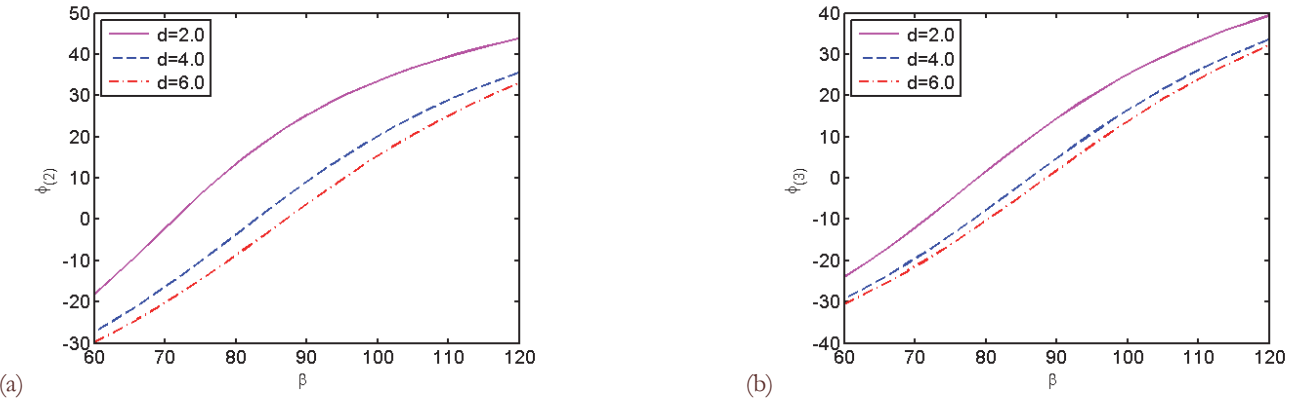


Figure 16: Fracture angles $\phi_{(1)}$ and $\phi_{(2)}$ as functions of the inclination angle $\beta=\beta_n$ of the edge cracks to the surface for different distances d between the cracks: (a) for crack 2 ($60^\circ \leq \beta \leq 120^\circ$), (b) for crack 3 ($60^\circ \leq \beta \leq 120^\circ$). Three edge cracks with different sizes $a_1=1$ and $a_2=a_3=0.5$. (For small angles the figures are similar to the case of two cracks.)

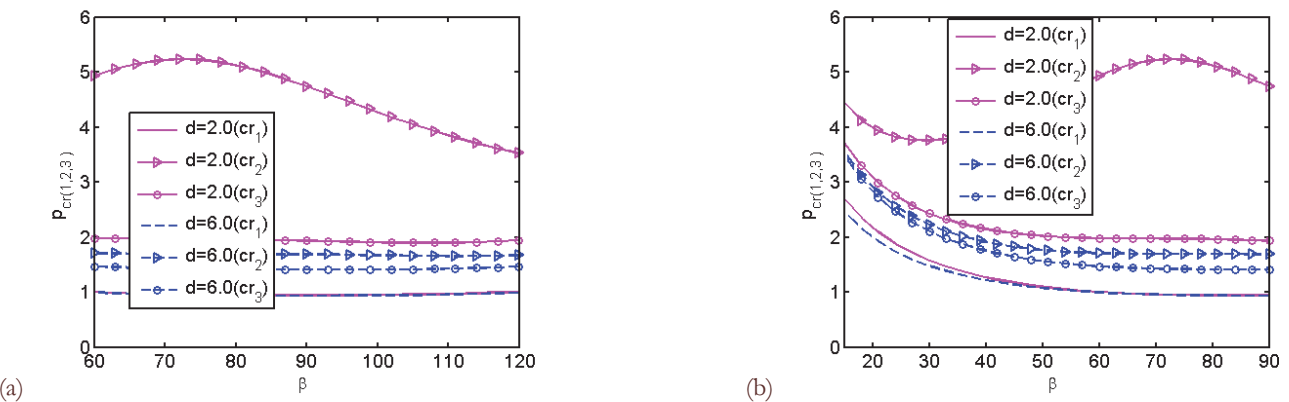


Figure 17: The non-dimensional critical load p_{cr} as function of the inclination angle $\beta=\beta_n$ for two equal edge cracks for different distances d between the cracks: (a) for 3 cracks ($60^\circ \leq \beta \leq 120^\circ$), (b) for 3 cracks ($20^\circ \leq \beta \leq 90^\circ$). Three edge cracks with different sizes $a_1=1$ and $a_2=a_3=0.5$.

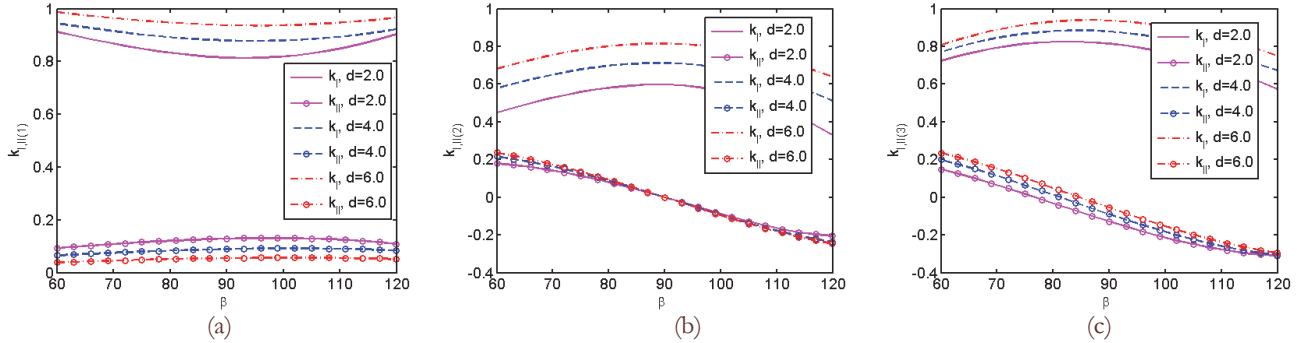


Figure 18: Stress intensity factors k_I and k_{II} as function of the inclination angle $\beta=\beta_2$ ($60^\circ \leq \beta \leq 120^\circ$) and for $\beta_1=90^\circ$ for different distances d between the cracks: (a) for crack 1, (b) for crack 2, (c) for crack 3. Three equal edge cracks.

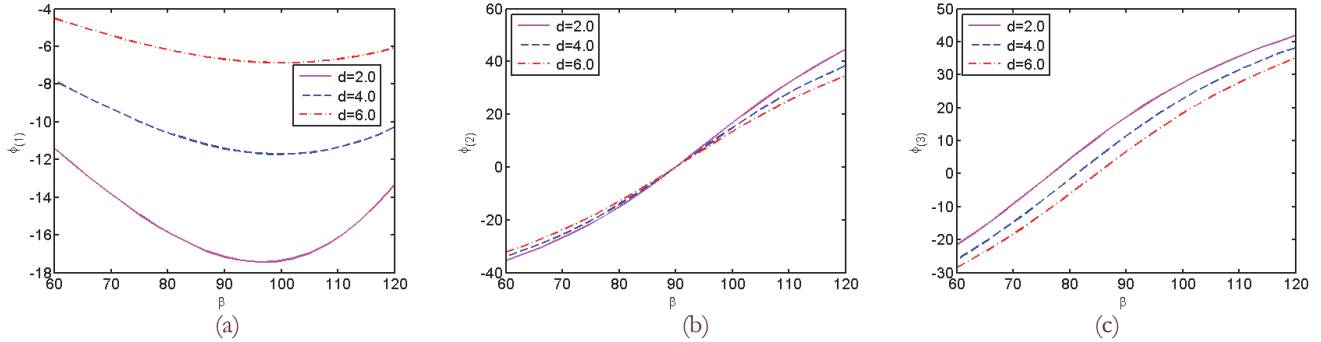


Figure 19: Fracture angles ϕ as functions of the inclination angle $\beta=\beta_{2,3}$ ($60^\circ \leq \beta \leq 120^\circ$) and for $\beta_1=90^\circ$ for different distances d between the cracks: (a) for crack 1, (b) for crack 2, (c) for crack 3. Three equal edge cracks.

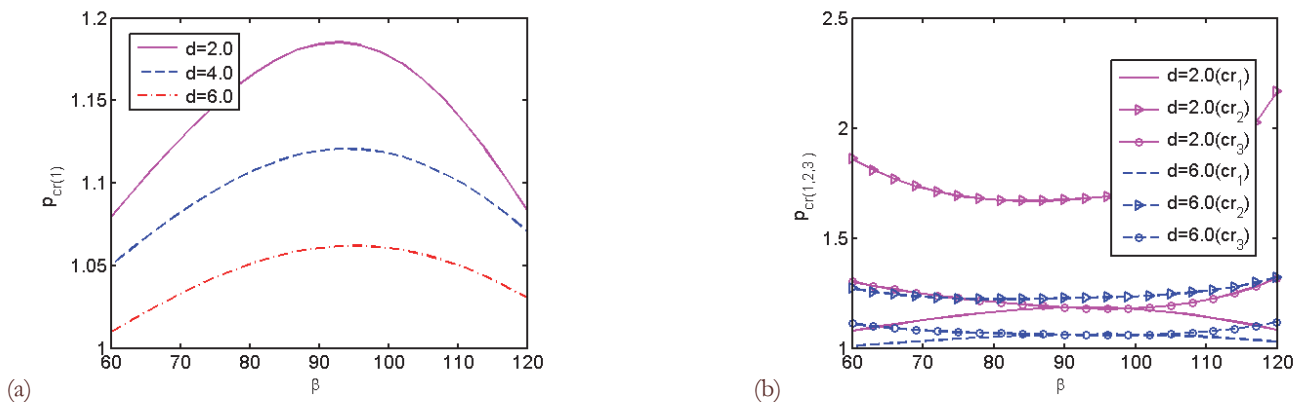


Figure 20: The non-dimensional critical load p_{cr} as function of the inclination angle $\beta=\beta_{2,3}$ ($60^\circ \leq \beta \leq 120^\circ$) and for $\beta_1=90^\circ$ for different distances d between the cracks: (a) for crack 1, (b) for 3 cracks. Three edge cracks same size.

Some schemes of the direction of cracks propagation for three cracks are shown in Fig. 21 and the results have been mentioned above. The schemes for fracture angles for other crack geometries can be built using the data in Figs. 13, 16 and 19.

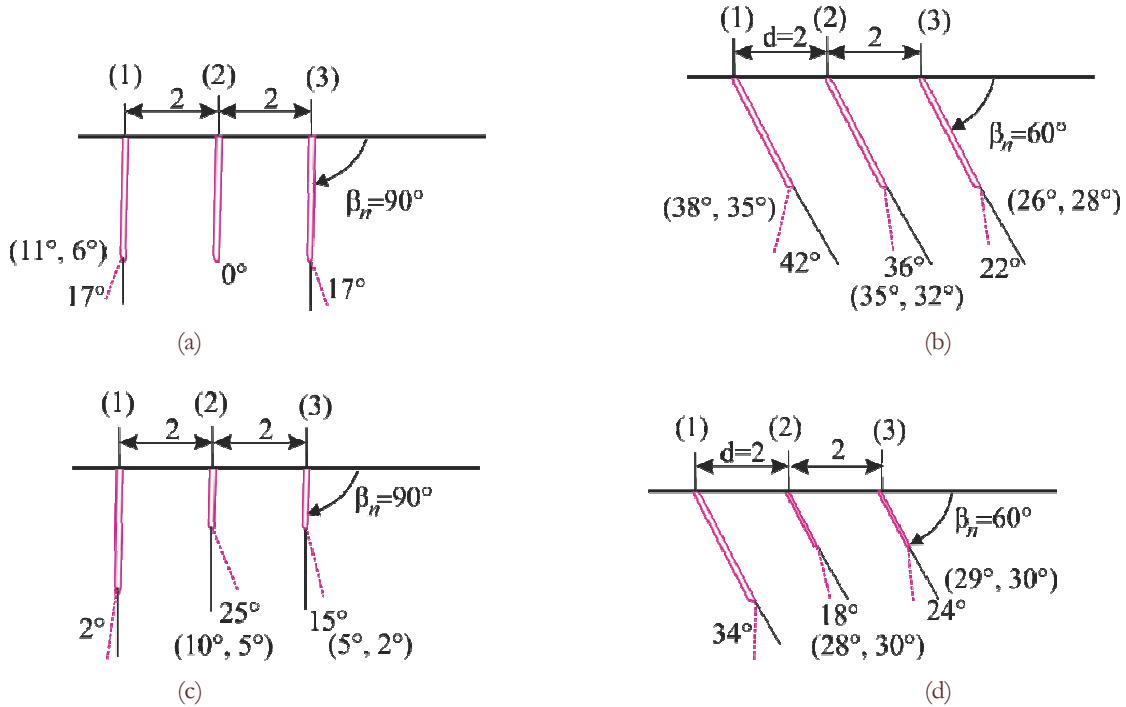


Figure 21: Schematic representation of the fracture angles: (a) and (b) for three equal cracks with inclined angles $\beta=90^\circ$ and 60° correspondingly; (c) and (d) for three crack of sizes $a_1=1$ and $a_2=a_3=0.5$ and with inclined angles $\beta=90^\circ$ and 60° .

Crack interaction effect

The shielding – amplification effects are observed in crack interaction problems, i.e. some geometries of the interacting cracks can enhance or suppress the propagation of each other. This problem has long history of discussion especially for macro-microcrack interaction problems [21]. In a recent paper by Wang et al [22] the authors return to this problem. The shielding and amplification effects of transverse array of microcracks on a main crack were investigated using extended FEM with respect to SIFs. The SIFs at the main crack tip include not only the interaction between the main crack and each of small cracks, but also include mutual interaction of microcracks. It was pointed out that the interaction between microcracks can weaken their amplification-shielding effect on the main crack and this effect was demonstrated in [22].

In the present problem for edge cracks we can check whether this interaction effect presents or not.

Consider the case of two edge cracks with sizes $(a_1, a_2)=(1.0, 0.5)$ and three edge cracks with sizes $(a_1, a_2, a_3)=(1.0, 0.5, 0.5)$, in both cases the cracks have same inclination angle β to the surface $\beta_n=\beta$.

Introduce the a notation

$$\Delta_1 = k_{I(1)} - k^0$$

for two cracks with distance between the cracks $d=2$ and for distance $d=4$

$$\Delta_2 = k_{I(2)} - k^0$$

and

$$\Delta_3 = k_{I(3)} - k^0$$

for 3 cracks with equal distances between the cracks $d=2$, where $k_{I(n)}$ is the SIF at the tip of large crack, k^0 is the SIF for a single edge crack. These values of Δ determine interaction effects between the cracks, i.e. the influence of small cracks on the large crack 1.

The value $\Delta_1 + \Delta_2 - \Delta_3$ will give the magnitude of mutual interaction of small cracks (crack 2 and 3) and

$$f = [(\Delta_1 + \Delta_2 - \Delta_3) / k^0] \times 100\%$$



is the relative value of this small crack interaction.

The data for SIFs are given in Tab. 2. SIF $k^0=0.92$ for a single crack with inclination angle $\beta=60^\circ$ can be found in [19] in Tab. 4 or in [11] in Tab. 1.

The SIF $k_I^{(1)}$ for crack 1 as influenced by a crack 2 on the distance $d=2$ is 1.094 and this value is less than SIF $k^0=1.12$ on the value $|\Delta_1|=0.026$ (first column in Tab. 2), and for the cracks on the distance $d=4$ the SIF $k_I^{(2)}=1.071$ is less than k^0 on $|\Delta_2|=0.05$ (second column in Tab. 2). The total interaction effect of the cracks 1 and 2 on the large crack 1 is $|\Delta_1 + \Delta_2|=0.076$ (if superposition of these interactions is assumed).

The SIF k_I for crack 1 under the influence of pair interacting cracks 2 and 3 is $k_I^{(3)}=1.061$ (distances between the cracks are $d=2$) and $|\Delta_3|=0.06$ is for this case. $|\Delta_3|$ is less than $|\Delta_1 + \Delta_2|$ on 0.016. That is, the solution to the problem of three edge cracks gives interaction effect on 0.016 less than the superimposed effect of two separate cracks derived from the problems of two-crack interaction. It is an example of calculations for $\beta=90^\circ$, for $\beta=60^\circ$ calculations are similar.

Tab. 2 in the last column show that the interaction between small cracks (crack 2 and 3) weaken the shielding effect on 1.5% for the cracks inclined on $\beta=90^\circ$ and on 2.17% for the cracks with $\beta=60^\circ$. It is rather small values, but, probably, for interaction of multiple cracks the effect will be stronger.

β	$d=2$ $k_I^{(1)}, \Delta_1$	$d=4$ $k_I^{(2)}, \Delta_2$	$d=2$ $k_I^{(3)}, \Delta_3$	$(\Delta_1 + \Delta_2) - \Delta_3$	k^0	$f\%$
90°	1.094, -0.026	1.071, -0.05	1.061, -0.06	-0.016	1.12	-1.5
60°	0.88, -0.04	0.86, -0.06	0.84, -0.08	-0.02	0.92	-2.17

Table 2: SIFs k_I at crack 1 interacting with small cracks and their interaction effects.

CONCLUSIONS

The effects of the interaction of edge cracks on further crack formation were studied with respect to main fracture characteristics, namely, stress intensity factors, fracture angles and critical loads. Some illustrative examples show the influence of inclination angles, distances between the cracks and sizes of the cracks on this interaction. The interaction of cracks leads to mixed mode conditions near the crack tips even for symmetric geometries and loading normal to the crack lines. As an illustration, a classical edge crack (i.e. the crack normal to the boundary and under tension normal to the crack line) in the presence of other crack is under mixed mode conditions and deviates from its initial propagation direction, albeit the other crack is small (Fig. 9 a and 11 c).

The crack shielding takes place (as expected for this problem) for most parameters of the problem. The maximum magnitude of the shielding effect is observed for close located cracks and for a middle crack in the case of the interaction of three cracks. The influence of two interacting cracks on the third crack can weaken the shielding effect and it was shown for SIF Mode I which is dominant in this problem.

The applied method of singular integral equations (which have been solved by well-known numerical method based on the quadratic formulas for integrals) in combination of a fracture criteria (the maximum hoop stress criteria has been used) is effective method for modeling of the crack interaction at the initial stage of their propagation.

ACKNOWLEDGEMENT

The support of the German Research Foundation under the grant Schm 746/139-1 is greatly acknowledged.

APPENDIX

In Eqs. (2) the kernels $R_{nk}(t,x)$ and $S_{nk}(t,x)$ are written as



$$\begin{aligned} R_{nk}(t, x) = & (1 - \delta_{nk}) K_{nk}(t, x) + \frac{e^{i\alpha_k}}{2} \left\{ \frac{1}{X_n - \bar{T}_k} + \frac{e^{-2i\alpha_n}}{\bar{X}_n - T_k} + \right. \\ & \left. + (\bar{T}_k - T_k) \left[\frac{1 + e^{-2i\alpha_n}}{(\bar{X}_n - T_k)^2} - \frac{2e^{-2i\alpha_n}(X_n - T_k)}{(\bar{X}_n - T_k)^3} \right] \right\} \end{aligned} \quad (\text{A.1})$$

$$S_{nk}(t, x) = (1 - \delta_{nk}) L_{nk}(t, x) + \frac{e^{-i\alpha_k}}{2} \left[\frac{T_k - \bar{T}_k}{(X_n - \bar{T}_k)^2} + \frac{1}{\bar{X}_n - T_k} - e^{-2i\alpha_n} \frac{X_n - T_k}{(\bar{X}_n - T_k)^2} \right] \quad (\text{A.2})$$

and the kernels $K_{nk}(t, x)$ and $L_{nk}(t, x)$ are

$$K_{nk}(t, x) = \frac{e^{i\alpha_k}}{2} \left(\frac{1}{T_k - X_n} + \frac{e^{-2i\alpha_n}}{\bar{T}_k - \bar{X}_n} \right) \quad (\text{A.3})$$

$$L_{nk}(t, x) = \frac{e^{-i\alpha_k}}{2} \left(\frac{1}{\bar{T}_k - \bar{X}_n} + \frac{T_k - X_n}{(\bar{T}_k - \bar{X}_n)^2} e^{-2i\alpha_n} \right) \quad (\text{A.4})$$

where

$$T_k = t e^{i\alpha_k} + z_k^0, \quad X_n = x e^{i\alpha_n} + z_n^0, \quad n, k = 1, 2, \dots, N \quad (\text{A.5})$$

and

$$\delta_{nk} = \begin{cases} 0 & \text{for } n \neq k; \\ 1 & \text{for } n = k. \end{cases}$$

The kernels $K_{nk}(t, x)$ and $L_{nk}(t, x)$ are the same as for the system of cracks in an infinite plane, and the additional terms in Eqs. (A.1) and (A.2) are responsible for the influence of the edge of the half plane. α_n is the inclination angle of n-th crack to the x-axis and $\alpha_n = -\beta_n$, Fig. 1; z_n^0 is the coordinate of the center of crack in global coordinate system (x, y).

REFERENCES

- [1] Anderson, T. L., Fracture Mechanics: Fundamentals and Applications, third ed., Taylor & Francis, (2005).
- [2] Daud, R., Ariffin, A. K., Abdullah, Sh., Ismail, Al E., Interacting cracks analysis using finite element method, in: A. Belov (Ed.), Applied Fracture Mechanics, InTech, (2012) 359 – 380. DOI: 10.5772/54358.
- [3] https://en.wikipedia.org/wiki/Crocodile_cracking.
- [4] Rangaraj, S., Kokini, K., Multiple surface cracking and its effect on interface cracks in functionally graded thermal barrier coatings under thermal shock, Trans. ASME J. Appl. Mech., 70 (2003), 234-245. DOI: 10.1115/1.1533809.
- [5] Kawasaki, A., Watanabe, R., Thermal fracture behavior of metal/ceramic functionally graded materials, Eng. Fract. Mech., 69 (2002) 1713–1728.
- [6] Gilbert, A., Kokini, K., Sankarasubramanian, S., Thermal fracture of zirconia-mullite composite thermal barrier coatings under thermal shock: An experimental study, Surf. Coat. Technol., 202(10) (2008), 2152-2161. DOI: 10.1016/j.surfcoat.2007.09.001.
- [7] Petrova, V., Schmauder, S., Thermal fracture of a functionally graded/homogeneous bimaterial with a system of cracks, Theor. Appl. Fract. Mech., 55 (2011) 148–157.
- [8] Petrova, V., Schmauder, S., Mathematical modelling and thermal stress intensity factors evaluation for an interface crack in the presence of a system of cracks in functionally graded/ homogeneous bimaterials, Comp. Mater. Sci., 52 (2012) 171-177. DOI:10.1016/j.commatsci.2011.02.028.



- [9] Petrova, V., Schmauder, S., Interaction of a system of cracks with an interface crack in functionally graded/homogeneous bimaterials under thermo-mechanical loading, *Comp. Mater. Sci.*, 64 (2012) 229–233. DOI: 10.1016/j.commatsci.2012.04.032.
- [10] Petrova, V., Schmauder, S., FGM/homogeneous bimaterials with systems of cracks under thermo-mechanical loading: Analysis by fracture criteria, *Eng. Fract. Mech.*, 130 (2014) 12–20. DOI: 10.1016/j.engfracmech.2014.01.014.
- [11] Petrova, V., Sadowski, T., Theoretical modeling and analysis of thermal fracture of semi-infinite functionally graded materials with edge cracks, *Meccanica* 49 (2014), 2603-2615. DOI: 10.1007/s11012-014-9941-x.
- [12] Zhou, B., Kokini, K., Effect of surface pre-crack morphology on the fracture of thermal barrier coatings under thermal shock, *Acta Mater.*, 52 (2004) 4189–4197. DOI: 10.1016/j.actamat.2004.05.035.
- [13] Feng, Y.Z., Jin, Z.-H., Thermal shock damage and residual strength behavior of a functionally graded plate with surface cracks alternating length, *J. Therm. Stresses*, 35 (2012) 30–47. DOI: 10.1080/01495739.2012.637457.
- [14] Afsar, A.M., Sekine, H., Crack spacing effect on the brittle fracture characteristics of semi-infinite functionally graded materials with periodic edge cracks, *Int. J. Fract.*, 102 (2000) L61-L66.
- [15] Panasyuk, V., Savruk, M., Datsyshin, A., Stress Distribution near Cracks in Plates and Shells (in Russian), Naukova Dumka, Kiev (1976).
- [16] Savruk, M.P., Two-Dimensional Problems of Elasticity for Body with Cracks (in Russian), Naukova Dumka, Kiev (1981).
- [17] Erdogan, F., Gupta, G., On the numerical solution of singular integral equations, *Quart. Appl. Math.*, 29 (1972) 525–534.
- [18] Erdogan, F., Sih, G.C., On the crack extension in plates under plane loading and transverse shear, *J. Basic. Eng.*, 85 (1963) 519–527.
- [19] Noda, N-A, Oda, K., Numerical solution of the singular integral equations in the crack analysis using the body force method. *Int. J. Fract.*, 58 (1992) 285-304. DOI: 10.1007/BF00048950.
- [20] Freese, C.E., Periodic edge cracks of unequal length in a semi-infinite tensile sheet. *Int J. Fract.*, 12 (1976) 125-134. DOI: 10.1007/BF00036015
- [21] Petrova, V., Tamuzs, V., Romalis, N., A survey of macro-microcrack interaction problems, *ASME Appl. Mech. Rev.*, 53 (2000) 117-146.
- [22] Wang, H., Liu, Z., Xu, D., Zeng, Q., Zhuang, Z., Chen, Z., Extended finite element method analysis for shielding and amplification effect of a main crack interacted with a group of nearby parallel microcrack, *Int. J. Damage Mech.*, 25 (1) (2016) 4-25. DOI: 10.1177/1056789514565933.